
Residual Connections Harm Generative Representation Learning

Xiao Zhang^{*1} Ruoxi Jiang^{*1} William Gao¹ Rebecca Willett^{1,2} Michael Maire¹

Abstract

We show that introducing a weighting factor to reduce the influence of identity shortcuts in residual networks significantly enhances semantic feature learning in generative representation learning frameworks, such as masked autoencoders (MAEs) and diffusion models. Our modification notably improves feature quality, raising ImageNet-1K K-Nearest Neighbor accuracy from 27.4% to 63.9% and linear probing accuracy from 67.8% to 72.7% for MAEs with a ViT-B/16 backbone, while also enhancing generation quality in diffusion models. This significant gap suggests that, while residual connection structure serves an essential role in facilitating gradient propagation, it may have a harmful side effect of reducing capacity for abstract learning by virtue of injecting an echo of shallower representations into deeper layers. We ameliorate this downside via a fixed formula for monotonically decreasing the contribution of identity connections as layer depth increases. Our design promotes the gradual development of feature abstractions, without impacting network trainability. Analyzing the representations learned by our modified residual networks, we find correlation between low effective feature rank and downstream task performance.

1. Introduction

Residual networks (ResNets) (He et al., 2016) define a connection structure that has achieved near-universal adoption into modern architectures for deep learning. At the time of their development, supervised learning (*e.g.*, ImageNet (Deng et al., 2009) classification) was the driving force behind the evolution of convolutional neural network (CNN) architectures. Residual networks solved a key issue:

^{*}Equal contribution ¹Department of Computer Science, The University of Chicago, Chicago, USA ²Department of Statistics, The University of Chicago, Chicago, USA. Correspondence to: Xiao Zhang <zhang7@uchicago.edu>, Ruoxi Jiang <roxie62@uchicago.edu>.

CNNs constructed of more than approximately 20 convolutional layers in sequence became difficult to train, leading to shallower networks outperforming deeper ones, unless additional techniques, such as auxiliary outputs (Szegedy et al., 2015) or batch normalization (Ioffe & Szegedy, 2015), were employed. Both ResNets, and their predecessor, highway networks (Srivastava et al., 2015a) provide elegant solutions to this trainability problem by endowing the network architecture with alternative shortcut pathways along which to propagate gradients. Highway networks present a more general formulation that modulates these shortcut connections with learned gating functions. However, given their sufficient empirical effectiveness, the simplicity of ResNet’s identity shortcuts makes them a preferred technique.

While solving the gradient propagation issue, residual connections impose a specific functional form on the network; between residual connections, each layer (or block of layers) learns to produce an update slated to be added to its own input. This incremental functional form may influence the computational procedures learned by the network (Greff et al., 2017). Alternatives to residual and highway networks exist that do not share this functional form, but implement other kinds of skip-connection scaffolding in order to assist gradient propagation (Larsson et al., 2017; Huang et al., 2017; Zhu et al., 2018). Thus, shortcut pathways, rather than a specific form of skip connection, are the essential ingredient to enable the training of very deep networks. Nevertheless, nearly all modern large-scale models, including those based on the transformer architecture (Vaswani et al., 2017) incorporate the standard residual connection.

This design choice holds, even as deep learning has shifted into an era driven by self-supervised training. The shift to self-supervision brings to the forefront new learning paradigms, including those based on contrastive (Wu et al., 2018; He et al., 2020; Chen et al., 2020; Caron et al., 2021; Grill et al., 2020), generative (Goodfellow et al., 2014; Karras et al., 2021; Ho et al., 2020; Song et al., 2021a; 2023; Rombach et al., 2022), and autoencoding (Kingma & Welling, 2013; He et al., 2022; Li et al., 2023) objectives. Many systems in the generative and autoencoding paradigms rely on “encoder-decoder” architectures, often styled after the original U-Net (Ronneberger et al., 2015), which contains additional long-range shortcuts between corresponding layers in mirrored symmetry about a central

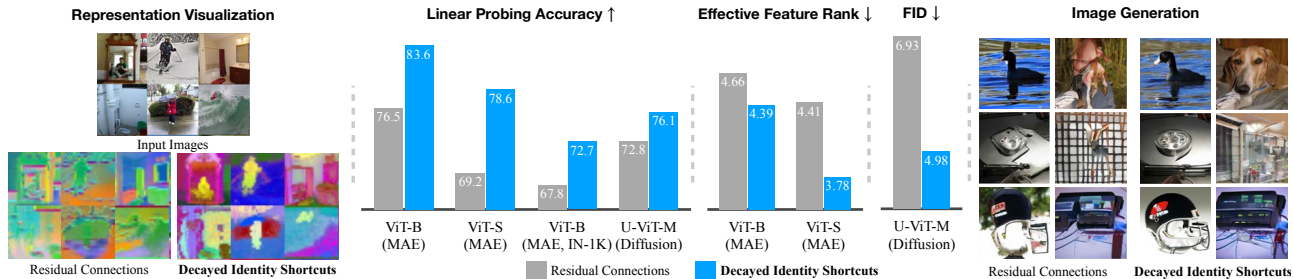


Figure 1. We design *decayed identity shortcuts* (Figure 2), a variant of residual connections, to facilitate self-supervised representation learning in generative model. Compared to standard residual connections, our approach yields superior abstract semantic features (left, visualized using Zhang et al. (2024)’s approach), whose leading components pop out object instances and classes. Quantitative evaluation shows our architecture encourages lower feature rank and learns better feature representation for both MAE and diffusion models (middle), along with enhanced generation quality for diffusion models (right). These improvements require no additional learnable parameters.

bottleneck. With representation learning as a goal, one typically desires that the middle bottleneck layer produce a feature embedding reflecting abstract semantic properties. The interaction of skip-connection scaffolding for gradient propagation with encoder-decoder architectures, self-supervised training objectives, and bottleneck representations has not been carefully reconsidered. This is a worrisome oversight, especially since, even in the supervised setting with standard classification architectures, prior work suggests that unweighted identity shortcuts may be a suboptimal design decision (Savarese & Figueiredo, 2017; Fischer et al., 2023).

Intuitively, identity shortcuts may not be entirely appropriate for capturing high-level, semantic features as they directly inject low-level, high-frequency details of inputs into outputs, potentially compromising feature abstraction. We explore this issue within generative learning frameworks, including masked autoencoders (MAEs) (He et al., 2022) and diffusion models (Ho et al., 2020), leading paradigms for self-supervised image representation learning and generation. Our experiments demonstrate that identity shortcuts significantly harm semantic feature learning in comparison to an alternative we propose: gradually decay the weight of the identity shortcut over the depth of the network, thereby reducing information flow through it (Figure 2). With increasing layer depth, our approach facilitates a smooth transition from a residual to a feed-forward architecture, while maintaining sufficient connectivity to train the network effectively. Unlike prior work on learned gating (Srivastava et al., 2015a) or reweighting (Savarese & Figueiredo, 2017) mechanisms for residual connections, our method is a forced decay scheme governed by a single hyperparameter.

A parallel motivation for our design stems from Huh et al. (2021), who show that features from residual blocks have higher rank than those produced by comparative feed-forward blocks. The smooth transition between residual and feed-forward behavior induced by our decay scheme regularizes deeper features toward exhibiting low-rank char-

acteristics. Section 6 experimentally explores the correlation between our decayed identity shortcuts and low-rank feature representations. Figure 1 previews the corresponding improvements to feature learning. Our contributions are:

- We introduce decayed identity shortcuts, a simple architectural mechanism which enhances feature abstraction in masked autoencoders and diffusion models.
- We identify a key correlation between our decayed identity shortcuts and low-rank inductive bias, empirically validating that our method improves classification accuracy and yields low-rank features.
- Our design within an MAE yields a substantial performance boost on ImageNet-1K (Deng et al., 2009): achieving a linear probing accuracy of 72.7% (up from a baseline of 67.8%) and a K-Nearest Neighbor accuracy of 63.9% (an improvement from the baseline of 27.4%).
- In diffusion models, our design improves both feature learning and generation quality.
- Smaller models with decayed identity shortcuts outperform larger ones using standard residual connections.

2. Related Work

Self-supervised representation learning. Recent advancements (Achiam et al., 2023; Kirillov et al., 2023; Rombach et al., 2022; Team et al., 2023; Shi et al., 2020; Ramesh et al., 2021) in deep learning follow a common scaling law, in which a model’s performance consistently improves with its capacity and the size of the training data. This effect can be observed in large language models (LLMs), which are trained on vast amounts of internet text, enabling them to perform some tasks at human level (Laskar et al., 2023) and exhibit remarkable zero-shot capabilities (Kojima et al., 2022). These models are trained using next-token-prediction, allowing them to be trained without labeled data. In contrast, the progress of this scaling law in computer

vision has largely depended on annotated data. For instance, the Segment Anything model (Kirillov et al., 2023) leverages 1 billion human-annotated masks, and state-of-the-art image generators (Ramesh et al., 2021) require training on huge datasets of text-image pairs (Schuhmann et al., 2022). However, the vast volume of unlabeled visual data and desire for continued scaling motivates a transition to self-supervised learning.

At present, two families of approaches to self-supervised visual representation learning appear particularly promising. **Contrastive representation learning** (Wu et al., 2018; He et al., 2020; Chen et al., 2020; Caron et al., 2021; Grill et al., 2020) achieves state-of-the-art performance in most downstream classification tasks by training discriminative models to maximize mutual information between differently augmented views of images. However, these approaches rely on extensive and intricate data augmentation pipelines, necessitating domain expertise for adaptation to new domains. **Generative representation learning**, via masked image modeling (Bao et al., 2022; He et al., 2022; Chen et al., 2024), which trains to reconstruct occluded pixels, or via diffusion denoising (Song et al., 2021b; Ho et al., 2020; Song et al., 2021a), which trains to reverse a process that mixes images with Gaussian noise, relying less on forming discriminative augmentations, learns to extract representations inherently along the generative process. Some hybrid approaches (Zhou et al., 2022; Huang et al., 2023; Li et al., 2023) combine both families. Despite advancements, neither has demonstrated the same scalability (Singh et al., 2023) as seen in LLMs. This challenge is additional motivation for reconsidering the foundations of self-supervised network architectures.

Residual and skip-connection architectures. Highway networks (Greff et al., 2017) first propose an additive skip connection structure to provide a scaffolding for gradient propagation when training very deep (e.g., 100 layer) networks. Motivated by the gating mechanisms within LSTMs (Hochreiter & Schmidhuber, 1997), this solution uses learned gating functions to weight each combination of identity and layer output branches. Residual networks (He et al., 2016) are a simplification that removes these learned coefficients. DenseNet (Huang et al., 2017) and FractalNet (Larsson et al., 2017) demonstrate that access to gradient paths of multiple lengths are the core requirement of training scaffolding, by introducing skip-connection structures with other functional forms. DenseNet utilizes feature concatenation instead of addition, while FractalNet imposes a recursive tree-like architecture combining subnetworks of multiple depths.

Zhu et al. (2018) explore variants of ResNets and DenseNets with fewer points of combination between different internal paths, demonstrating that a sparser scaffolding structure

may be more robust as network depth increases to thousands of layers. Savarese & Figueiredo (2017) add a scalar gating functional to the layer output in residual networks, yielding a hybrid design between residual and highway networks; learning this scalar gating provides a consistent benefit to classification accuracy. Fischer et al. (2023) develop a weighting scheme for residual connections based upon a sensitivity analysis of signal propagation within a ResNet. To date, none of these potential improvements have seen broad adoption.

Low rank bias in neural networks. Over-parameterized neural networks exhibit surprising generalization capabilities, a finding seemingly in contradiction with classical machine learning theory (Neyshabur et al., 2019). This phenomenon implies the existence of some form of implicit regularization that prevents the model from overfitting. From the perspective of neural network parameterizations, Arora et al. (2019) suggest that linear models with more layers tend to converge to minimal norm solutions. In the context of CNNs, Huh et al. (2021) demonstrate that stacking more feed-forward layers compels the model to seek lower rank solutions, and Jing et al. (2020) reinforce this finding by adding more layers to an autoencoder’s bottleneck, thereby creating a representation bottleneck. In vision transformers, Geshkovski et al. (2024) examine the connection between attention blocks and mean-shift clustering (Cheng, 1995), showing that repeated attention operations result in low-rank outputs. Moreover, Dong et al. (2021) reveal that eliminating the shortcut connection from residual attention blocks causes features to degenerate to rank 1 structures doubly exponentially. From a different perspective, recent work (Radhakrishnan et al., 2022; Beaglehole et al., 2023; Radhakrishnan et al., 2024) shows training algorithms implicitly induce low-rank behavior in neural networks. Radhakrishnan et al. (2024) study the dimensionality reduction behavior of a recursive feature machine (Radhakrishnan et al., 2022) and effectively verify performance on low-rank matrix recovery.

3. Method

Prior works show that deeper feed-forward architectures have an inductive bias towards producing low-rank feature maps, while ResNets do not display the same behavior (Huh et al., 2021). However, despite this bias, deeper feed-forward architectures are typically less effective and generalize worse than ResNets (He et al., 2016). We aim to combine the properties of both feed-forward networks and ResNets, using the low-rank prior to enhance the abstraction capability of the network while maintaining the core benefits of the residual block, including stable training and the capacity to construct deeper models.

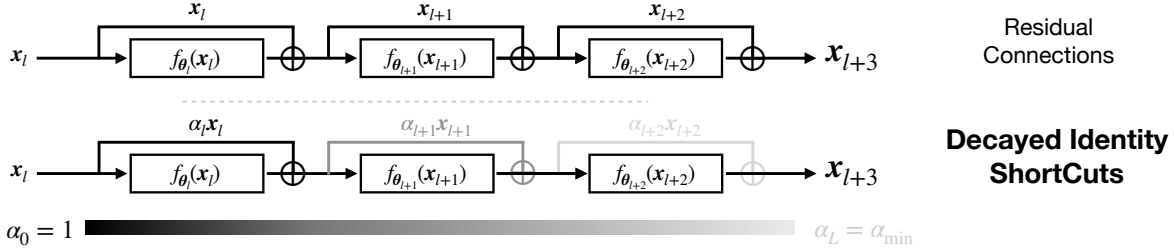


Figure 2. Our *decayed identity shortcuts* introduce a depth-dependent scaling factor to shortcuts in a residual network, thereby modulating the contribution of preceding layers and fostering greater abstraction in deeper layers. A simple schema for controlling decay factor α suffices to improve feature learning in both MAEs and diffusion models, as well as diffusion model generation quality.

3.1. Decayed Identity Shortcuts

Feed-forward layers. Consider a neural network of L layers. For each layer l parameterized with θ_l , the operation of a feed-forward neural network can be described as:

$$\mathbf{x}_{l+1} = f_{\theta_l}(\mathbf{x}_l), \quad (1)$$

where $\mathbf{x}_l \in \mathbb{R}^d$ represents the output from the preceding layer, and f_{θ_l} denotes the network block applied at the current layer. Although it is widely known that pure feed-forward architectures are susceptible to vanishing gradients when building deeper models, Huh et al. (2021) demonstrates that feed-forward modules offer implicit structural regularization, enabling deep models to generate abstract representations at bottlenecks.

Residual connections. To address the optimization problem of vanishing gradients in deeper neural networks, ResNets (He et al., 2016) construct each layer as a residual function, resulting in a modification to Eq. 1:

$$\mathbf{x}_{l+1} = \mathbf{x}_l + f_{\theta_l}(\mathbf{x}_l). \quad (2)$$

This design builds shortcuts from input to output, allowing gradient magnitude to be preserved regardless of the depth of the model. However, a consequence of this design is that the output stays close to the input in practice (Greff et al., 2017), defeating the need to construct complex transformations over depth. The same phenomenon is also observed in highway networks (Srivastava et al., 2015a), which adopt learnable gates $H_\phi(\mathbf{x}) \in [0, 1]^d$ in both the residual and skip branches: $\mathbf{x}_{l+1} = H_\phi(\mathbf{x}_l) \cdot \mathbf{x}_l + (1 - H_\phi(\mathbf{x}_l)) \cdot f_{\theta_l}(\mathbf{x}_l)$. Although this flexible design allows the model to build the abstraction level over depths, similar to feedforward networks, Srivastava et al. (2015b) finds $H_\phi \approx 1$ for most units, suggesting the model prefers copying the input.

Decayed identity shortcuts for unsupervised representation learning. Setting aside the optimization benefits brought by residual connections, we rethink the role of the residual connections from the viewpoint of representation learning. Abstraction can be viewed as invariance to local changes of input and is crucial to the disentanglement of

the feature space (Bengio et al., 2013). Prior work suggests that a shortcut path of residual connections tends to preserve high-frequency fine-grained input information (Greff et al., 2017), resulting in decreased feature abstraction. We hypothesize that this lack of abstraction harms the capability of the model to learn meaningful low-level features and that ensuring an abstract structure in the deeper layers of the neural network will help improve representation learning, especially for unsupervised tasks that often use indirect proxy objectives, such as pixel-wise reconstruction loss. Motivated by this hypothesis, we propose to downweight the contribution from the shortcut path:

$$\mathbf{x}_{l+1} = \alpha_l \mathbf{x}_l + f_{\theta_l}(\mathbf{x}_l), \quad (3)$$

where $\alpha_l \in [0, 1]$ is a rescaling factor to the residual path, controlling the information flow through the skip connection. Fully expanding this relation for a network with L layers indexed from 1 to L , we have that:

$$\mathbf{x}_{L+1} = \left(\prod_{l=1}^L \alpha_l \right) \mathbf{x}_0 + \sum_{l=1}^{L-1} \left(\prod_{i=l+1}^L \alpha_i \right) f_{\theta_l}(\mathbf{x}_l) + f_{\theta_L}(\mathbf{x}_L). \quad (4)$$

We see that the contribution of the input \mathbf{x}_0 is scaled by each $\alpha_l \leq 1$ while each subsequent network block output $f_{\theta_l}(\mathbf{x}_l)$ omits scaling factors up to α_l . Hence, the contribution of early features of the network is especially down-weighted, preventing the network from passing fine-grained detailed information to the bottleneck X_{L+1} . During our experiments, we find the effective decay factor of the final layer, $\alpha_L^{\text{eff}} = \prod_{l=1}^L \alpha_l$, plays a critical role in deciding the optimal decay rate when varying the network depth L .

Decay schema. Instead of specifying α_l as a constant across all layers, we choose α_l to be a function parameterized by the layer index l , where the contribution from the shortcut path is monotonically decreasing when l increases:

$$\alpha_l = 1 - \delta_\alpha l, \quad (5)$$

where $\delta_\alpha := \frac{(1-\alpha_{\min})}{L}$, $\alpha_L \equiv \alpha_{\min}$ is a minimum scaling factor applied at the final layer L . Our formulation brings

two primary benefits. First, α_l , as a linear interpolation between 0 and 1, acts as a smooth transition between residual connections and feedforward layers, bringing us the optimization benefits seen in the residual connections, while simultaneously encouraging learning the deeper layers to learn more abstract representations. Second, similar to the naive formulation, our method only introduces one extra hyperparameter α_{\min} , which is not data-dependent and does not need to be learned.

3.2. Implementation Strategy

Skip connections for autoencoders. Since our method progressively decays the residual connections over network depth, it encourages the most abstract features to be learned by later layers. However, learning an abstract bottleneck is detrimental to the training objectives that aim for pixel-wise reconstruction, as they necessitate the preservation of detailed information. To address this, we incorporate standard skip connections between the encoder and decoder, enabling the encoder to directly pass information from shallow layers to the decoder while learning increasingly abstract representations in the deeper encoder layers.

Stabilizing training with residual zero initialization. The model exhibits rapid feature norm growth at the beginning of training for $\alpha_{\min} \leq 0.7$. We suspect that the model learns to amplify the output feature norm of $f_{\theta_l}(x)$ to counteract the significant decay applied to the residual connection. This growth leads to training instability and negatively impacts training convergence. To address this issue, we follow the implementation of previous works (Ho et al., 2020) and initialize the weights of the final output layer in each f_{θ_l} to zero instead of using the original Xavier uniform initialization (Glorot & Bengio, 2010). This approach enhances training stability by controlling the growth of feature norm, especially with smaller α_{\min} .

4. Experiments on Masked Autoencoder (MAE)

For masked autoencoders (MAEs) (He et al., 2022), we replace the residual connections in the encoder’s MLP and attention blocks with decayed identity shortcuts. The MAE operates by accepting images with a random subset of pixels masked out and learning to recover the discarded pixels. Since the original MAE has twice the number of encoder layers as decoder layers, we build encoder-decoder skip connections by injecting output from every other encoder layer into the corresponding decoder layer. To match spatial dimensions, injected encoder features are combined with learnable masked tokens before channel-wise concatenation. The implementation details for the training and evaluation are shown in Section A. He et al. (2022) show the desired representations appear at the end of encoder; we therefore

Method	FT	LP	KNN
<i>Contrastive representation learning</i>			
MoCo-v3(Chen et al., 2021a)	83.2	76.7	66.6
DINO(Caron et al., 2021)	83.3	78.2	76.1
Con MIM(Yi et al., 2023)	83.7	39.3	-
<i>Generative representation learning</i>			
Data2Vec(Baevski et al., 2022)	84.2	68.0	33.2
I-JEPA(Assran et al., 2023)	-	72.9	-
CAE(Chen et al., 2024)	83.8	70.4	51.4
ADDP(VIT-L) (Tian et al., 2024)	85.9	23.8	-
Latent MIM(Wei et al., 2024)	83.0	72.0	50.1
MAE(He et al., 2022)	83.6	67.8	27.4
Ours ($\alpha_{\min} = 0.6$)	82.9	72.7	63.9

Table 1. **Benchmark of representations on the ImageNet-1K.** Evaluate learned features using standard evaluation protocols: linear probing (LP), fine-tuning (FT) and K-Nearest Neighbor (KNN). With only a simple architectural modification to MAE (He et al., 2022) and trained purely with pixel-wise reconstruction loss, we achieve 72.7% LP accuracy and 63.9% KNN accuracy, significantly narrowing down the gap between generative and contrastive representation learning frameworks

apply our decaying schema only to the encoder.

4.1. Representation Learning on ImageNet-1k

We follow the default hyperparameters from MAE (He et al., 2022) to pretrain ImageNet-1K train split (Deng et al., 2009) and use the standard protocol to evaluate the learned representation with end-to-end finetuning (FT), linear probing (LP) and K-Nearest Neighbour (KNN, $K = 20$), for image classification task. Please see the appendix for detailed experimental setups.

We report the results in Table 1. In the top half of the table, we present methods that employ a contrastive loss. Although these methods produce the best probing accuracies, their success depends on a carefully designed data augmentation process, which may need to be tuned for each different data distribution. In the bottom half, we show several methods based on generative architecture. Our method simply extends MAE by constructing an implicit feature bottleneck and shows significant improvements over the MAE baselines for both linear probing (72.7% vs. 67.3%) and K-Nearest Neighbour (63.9% vs. 27.4%). outperforming Data2Vec, Latent MIM and CAE and giving a probing accuracy competitive with I-JEPA, without needing to use explicit feature alignment.

End-to-end fine-tuning (FT), unlike linear probing which only trains a single linear layer, updates the entire network for image classification. Since the features can shift significantly from their pre-training state during end-to-end updating, we argue that this may not accurately reflect the quality of the learned representations. For example, DINO demonstrates superior performance in various downstream

Residual Connections Harm Generative Representation Learning

Feat. Dim.	Enc. Depth (L)	α_{\min}					α_L^{eff}			
		0.6	0.7	0.8	0.9	1.0 (Baseline)	(0, 1e-3)	[1e-3, 1e-2)	[1e-2, 1e-1)	[1e-1, 1]]
384	12	78.5	78.1	75.2	73.5	69.2	-	78.5	78.1	75.2
768	12	83.6	81.8	79.8	79.2	76.5	-	83.6	81.8	79.8
1024	12	83.2	82.5	82.1	79.3	78.0	-	83.2	82.5	82.1
768	18	83.5	85.0	84.4	81.8	79.2	78.5	85.0	84.4	81.8
1024	24	84.3	86.0	84.5	84.3	81.4	82.4	86.0	-	84.3

Table 2. **Linear Probing accuracy of MAE on ImageNet-100 varying α_{\min} and architecture size.** We show our method consistently improves the performance across all configurations. We notice the encoder depth rather than feature dimension influences the optimal α_{\min} . We attribute this behavior to the scaling effect of the input data to encoder’s final layer, quantified as $\alpha_L^{\text{eff}} = \prod_{l=1}^L \alpha_l$. Deeper model requires larger α_{\min} to maintain a consistent cumulative decay effect and we find setting α_{\min} such that $\alpha_L^{\text{eff}} \in [1e-3, 1e-2]$ yield the best performance. With our strategy, smaller model (768 feature dim + 12 layer) outperforms bigger one (1024 feature dim + 24 layer) with standard residual connections.

α_{\min}	α_l scheduler	UNet	LP
0.6	Linear	Yes	83.6
0.6	Linear	No	61.5
0.6	Cosine	Yes	82.8
0.7	Linear	Yes	81.8
0.7	Cosine	Yes	82.9
-	Learnable α_l	Yes	79.5

(a) **Effect of Skip Connections and α_l scheduler.** Skip connection is critical for performance. The choice of schedulers has less impact and learnable α_l is worse than pre-fixed α_l .

Configurations	Decay Block	α_{\min}	LP
$\mathbf{x}_{l+1} = \mathbf{x}_l + f_{\theta_l}(\mathbf{x}_l)$	-	-	76.5
$\mathbf{x}_{l+1} = \mathbf{x}_l + \sqrt{0.5}f_{\theta_l}(\mathbf{x}_l)$	MLP & Atten.	-	76.9
$\mathbf{x}_{l+1} = \sqrt{0.5}(\mathbf{x}_l + f_{\theta_l}(\mathbf{x}_l))$	MLP & Atten.	-	82.6
$\mathbf{x}_{l+1} = \alpha_l \mathbf{x}_l + f_{\theta}(\mathbf{x}_l)$	Atten.	0.6	79.3
$\mathbf{x}_{l+1} = \alpha_l \mathbf{x}_l + f_{\theta}(\mathbf{x}_l)$	MLP	0.6	80.6
$\mathbf{x}_{l+1} = \alpha_l \mathbf{x}_l + f_{\theta}(\mathbf{x}_l)$	MLP & Atten.	0.6	83.6

(b) **Other Decay Schemas.** We conduct ablations using a variety of scalings of the residual connection and observe that our design produces the best results.

Table 3. **Ablation experiments of MAE using ViT-B/16 in ImageNet-100.** We report the results with linear probing (LP) accuracy.

vision tasks compared to MAE, but its fine-tuning performance is worse than MAE. Similarly, ConMIM and ADDP exhibit poor linear probing performance, suggesting lower-quality representations, yet their fine-tuning performance surpasses that of contrastive learning methods. Nevertheless, we still provide the fine-tuning results for reference.

4.2. Ablation Studies on ImageNet-100

We conduct ablations on several properties of our framework on ImageNet-100. A summary of results can be found in Tables 2 and 3.

Decay rate α_{\min} . The only parameter of our framework is α_{\min} , the minimum scaling factor applied to the final layer. In Table 2, we show linear probing scores for varying values of α_{\min} . We observe that $\alpha_{\min} \in [0.6, 0.7]$ works well for most cases. If α_{\min} is too small, for example, $\alpha_{\min} \leq 0.4$, we observe that the training becomes unstable.

Architecture size. In Table 2, we also run experiments over multiple architecture choices. We notice encoder depth L rather than feature dimension that influences the optimal choices of α_{\min} and deeper models requires larger α_{\min} . We attribute this phenomenon to the cumulative decaying effect of the final layer, quantified as $\alpha_L^{\text{eff}} = \prod_{l=1}^L \alpha_l$. Heavy decaying would harm the optimization and selecting α_{\min} such that $\alpha_L^{\text{eff}} \in [1e-3, 1e-2]$ yields the best performance.

Skip connections. Another critical design choice in our network is to include skip connections that are not in the

original MAE. As discussed in Section 3.2, if the MAE does not use skip connections, the bottleneck layer must preserve all information to reconstruct the input image accurately. This is opposed to learn abstract representations at bottleneck. These contrary effects significantly degrade the representation learned by the model, leading to a 22.1% drop in the linear probing score, as we report in Table 3a.

α_l Scheduler. We use linear scheduler $\alpha_l = 1 - \frac{(1-\alpha_{\min})}{L}l$ as a default choice. In table 3a, we also experiment with a cosine scheduler but find it leads to worse performance for $\alpha_{\min} = 0.6, 0.7$. Besides using a prefixed α_l scheduler, we also experiment with a learnable α_l , which resembles the setup of highway network (Srivastava et al., 2015a). We show the learnable α_l at each layer in Table 5, appendix. From the table, we don’t find consistent patterns over network depth and the performance is worse than our pre-defined α_l scheduler.

Different decay schema. We also explore decay schema, with results summarized in Table 3b: (1) Scaling both branches of the residual blocks simultaneously by applying a constant factor, $\alpha = \sqrt{0.5}$, to both \mathbf{x} and $f_{\theta_l}(\mathbf{x})$. (2) Scaling only f_{θ_l} using the same constant factor, $\alpha = \sqrt{0.5}$. (3) Applying our proposed schema exclusively to either the attention or MLP branch.

Among these, (2) shows no significant improvement over the baseline, while (1) yields some improvement but still underperforms compared to our approach. By analyzing (1) and (2), we demonstrate that the representation gains are due to

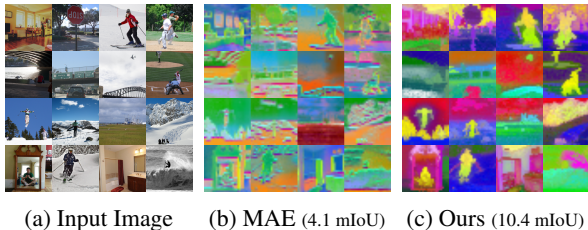


Figure 3. Visualize learned representations using Zhang et al. (2024) without cherry-picking. We project the learned representations onto a 3-channel feature map, visualized as RGB images. Our method learns more abstract and semantically consistent representations compared to the baseline MAE. This visual comparison is further supported by benchmarking on unsupervised semantic segmentation tasks, where our approach achieves better results (10.4 mIoU) compared to the baseline MAE (4.1 mIoU).

down-weighting the skip connection branch. Notably, recent diffusion models (Karras et al., 2018; Song et al., 2021b) have employed (1) in their smaller convolutional neural network but don’t provide systemic analysis. However, applying decay only to the MLP or attention branch reduces the overall decaying effect across the network, resulting in lower performance compared to our schema, which achieves the best performance among the tested designs.

4.3. Embedding analysis

We qualitatively evaluate the feature learning in Figure 3 and we adopt the pixel-wise embedding approaches proposed by Zhang et al. (2024) to group the representations from the last layer of the encoder into a lower dimensional space. We use their default hyperparameters to cluster representations across COCO validation set and render the top 3 eigenvectors as RGB channels of images. From the visualization, ours learns abstract representation and the object from the same categories have similar color, indicating a global consistent semantic grouping. The baseline MAE, on the other hand, doesn’t show clearly global semantic patterns.

We also benchmark the clustering quantitatively, following the postprocessing protocol (Zhang et al., 2024) to produced unsupervised semantic segmentation and report the results as the mean intersection of union (mIoU). Ours (10.41 mIoU) achieve 6.31 mIoU improvement over baseline (4.10 mIoU), which support the visual comparison.

5. Experiments on Diffusion Models

Diffusion models. We use U-ViT (Bao et al., 2023), a ViT-based diffusion model with skip connections between the encoder and decoder, as the baseline for our diffusion model experiments. Recent studies (Yang & Wang, 2023; Baranchuk et al., 2022) suggest that diffusion models learn

the best semantic representations near the decoder’s latter stages. Therefore, we apply our proposed decay mechanism up to the end of the decoder. While this design might be suboptimal, as the smallest decay factor may not align with the layers holding the best semantic representations, we demonstrate in practice that this simple approach effectively enhances both the learned representations and the quality of generated outputs.

Experimental details. We utilize the default scheduler and sampler from U-ViT (Bao et al., 2023), replacing only the residual connections with our proposed decayed shortcut connections. We train unconditional diffusion models on CIFAR-100 and ImageNet-100 without using image class labels. Additionally, we train a class-conditional diffusion model on ImageNet-100 to validate our design across different tasks. For ImageNet-100, instead of training directly on pixels, we adopt a latent diffusion (Rombach et al., 2022) approach by running the model in the latent space of a pretrained VAE, which reduces input resolutions from 256x256x3 to 32x32x4. We use U-ViT-Mid for ImageNet-100 and U-ViT-small for CIFAR-100. For model and training details, please refer to Bao et al. (2023).

We evaluate the learned representations with linear probing and we train a linear classifier over the frozen representations. We report the results as the best configurations, including the choices of layer index and noise level, that yields the best performance

Results. Our results are presented in Table 4, where we demonstrate that replacing residual connections with our proposed decayed identity shortcuts consistently enhances representation quality and image generation across both datasets and tasks (conditional and unconditional generation). Notably, this improvement is achieved without introducing any additional learnable parameters. We provide the visualization of generated images in the appendix for qualitative comparisons (Figure 8).

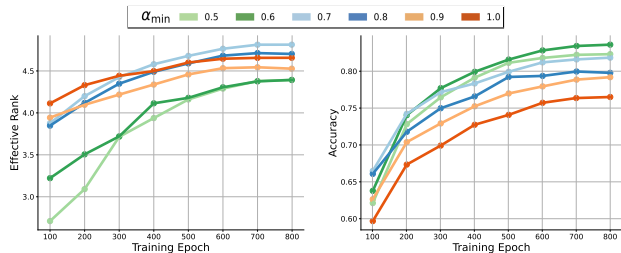
6. Discussion on feature rank

In this section, we try to answer a key question: How and why do residual connections impact the abstraction level of the deeper layers in a neural network? We delve deeper into how our design reinforces the low-rank bias of neural networks and try to connect our method to ideas in existing works (Huh et al., 2021). To this end, we visualize the training dynamics of our method and analysis the feature rank of our approach to provide a holistic analysis.

Low-rank simplicity bias. Huh et al. (2021) investigate the low-rank simplicity bias in deeper feed-forward neural networks, which drives neural networks to find low-rank solutions. At the same time, they make an empirical observation that deeper residual networks do not show a similar

Dataset	α_{\min}				Linear Probing (Acc.) \uparrow				Generation quality (FID) \downarrow			
	1.0	0.8	0.7	0.6	1.0	0.8	0.7	0.6	1.0	0.8	0.7	0.6
CIFAR-100 (Uncon.)	62.47	63.58	66.86	64.63	14.34	11.65	8.99	11.71				
ImageNet-100 (Uncond.)	72.8	74.5	76.1	75.8	44.40	40.96	41.17	43.51				
ImageNet-100 (Class Cond.)	-	-	-	-	6.93	5.75	5.11	4.98				

Table 4. **Performance using diffusion models.** In diffusion models, we demonstrate that our proposed decayed identity shortcut (with $\alpha_{\min} < 1.0$) enhances probing accuracy and improves generation quality across various datasets and configurations in both classes conditional and unconditional setups.



(a) Effective Rank of MAE over training epochs. (b) Linear probing accuracy of MAE over training epochs.

Figure 4. For MAE pretrained on ImageNet-100, we present visualizations of (a) the training dynamics of the effective rank for different values of α_{\min} , (b) the linear probing accuracy for various α_{\min} , demonstrating that a lower effective feature rank is associated with better performance.

rank contracting behavior.

Effective rank. For analysis purpose, Huh et al. (2021) quantify the rank of the learned representation using the *effective rank*, which is a continuous measure. For a matrix $\mathbf{A} \in \mathbb{R}^{m \times n}$, the effective rank $\rho(\mathbf{A})$ is defined as the Shannon entropy of the normalized singular values (Roy & Vetterli, 2007):

$$\rho(\mathbf{A}) = - \sum_i^{\min(n,m)} \bar{\sigma}_i \log \bar{\sigma}_i, \quad (6)$$

where $\bar{\sigma}_i = \sigma_i / \sum_j \sigma_j$ denotes the i^{th} normalized singular value. Intuitively, $\rho(\mathbf{A})$ is small when a few singular values dominate and large when singular values are evenly spread, hence giving a good continuous approximation for matrix rank. In the following subsections, we use the singular values from the covariance matrix \mathbf{A}_θ of the last-layer features to compute $\rho(\mathbf{A})$, where $\mathbf{A}_\theta(i, j)$ denotes the covariance of the learned class tokens for the i^{th} and j^{th} samples.

Inspired by Huh et al. (2021), we conjecture that the improvement to feature learning capability of our method can mainly be attributed to the decayed identity shortcuts promoting low-rank features at the bottleneck. In Figures 4a and 4b, we measure the training dynamics of the models (feature dimension 768 and encoder depth 12) in terms of accuracy and the effective rank, for different values of α_{\min}

During the early epochs, models with lower α_{\min} tend to exhibit both lower effective rank and higher probing accuracy, supporting our hypothesis. As training progresses, the correlations between α_{\min} and effective rank become less precise. We suspect this is due model’s effort to compensate for the decay factors with large decaying factor. Despite this, we can still conclude that lower $\alpha_{\min} = [0.5-0.6]$ results in lower feature rank and better probing accuracy compared to higher $\alpha_{\min} = [0.7-1.0]$.

Compatibility with contrastive learning frameworks.

Despite substantial improvement of applying our decayed identity shortcuts in generative model, we note that our approach does not easily extend to contrastive learning frameworks, where the low rank inductive bias conflicts with the training objectives, e.g., MoCov3 (Chen et al., 2021b) include an universal repulsive term in the denominator to increase the feature rank. Rankme (Garrido et al., 2023) confirms this by showing conservative learning models with higher feature ranks yield better results.

7. Conclusion

Huh et al. (2021) raise a key insight in their work – that how a neural network is parameterized matters for fitting the data – and investigate the inductive low-rank bias of stacking more linear layers in a network. In this work, we observe that the ubiquitous residual network (He et al., 2016) may not be the ideal network parametrization for representation learning and propose a modification of the shortcut path in residual blocks that significantly improves unsupervised representation learning. We explore the connection between our reparameterization of the residual connection and the effective rank of the learned features, finding a correlation between good representations and low-rank representations.

Our work calls into question a fundamental design choice of neural networks that has been used in many modern architectures. By rethinking this choice, the door is open for further reparameterizations and improvements to unsupervised representation learning. The results we show provide a prompt for more extensive investigations into the connection between low effective rank and high-quality abstract representations, as well as the exploration of underlying theoretical mechanisms for this relationship.

8. Impact Statements

This paper presents work whose goal is to advance the field of generative representation learning. There are many potential societal consequences of our work, none of which we feel must be specifically highlighted here.

References

- Achiam, J., Adler, S., Agarwal, S., Ahmad, L., Akkaya, I., Aleman, F. L., Almeida, D., Altenschmidt, J., Altman, S., Anadkat, S., et al. GPT-4 technical report. *arXiv:2303.08774*, 2023.
- Arora, S., Cohen, N., Hu, W., and Luo, Y. Implicit regularization in deep matrix factorization. In *NeurIPS*, 2019.
- Assran, M., Duval, Q., Misra, I., Bojanowski, P., Vincent, P., Rabbat, M., LeCun, Y., and Ballas, N. Self-supervised learning from images with a joint-embedding predictive architecture. In *CVPR*, 2023.
- Baevski, A., Hsu, W.-N., Xu, Q., Babu, A., Gu, J., and Auli, M. Data2vec: A general framework for self-supervised learning in speech, vision and language. In *ICML*, 2022.
- Bao, F., Nie, S., Xue, K., Cao, Y., Li, C., Su, H., and Zhu, J. All are worth words: A ViT backbone for diffusion models. In *CVPR*, 2023.
- Bao, H., Dong, L., Piao, S., and Wei, F. BEiT: BERT pre-training of image transformers. In *ICLR*, 2022.
- Baranchuk, D., Rubachev, I., Voynov, A., Khrlukov, V., and Babenko, A. Label-efficient semantic segmentation with diffusion models. In *ICLR*, 2022.
- Beaglehole, D., Radhakrishnan, A., Pandit, P., and Belkin, M. Mechanism of feature learning in convolutional neural networks. *arXiv:2309.00570*, 2023.
- Bengio, Y., Courville, A., and Vincent, P. Representation learning: A review and new perspectives. *TPAMI*, 2013.
- Caron, M., Touvron, H., Misra, I., Jégou, H., Mairal, J., Bojanowski, P., and Joulin, A. Emerging properties in self-supervised vision transformers. In *ICCV*, 2021.
- Chen, T., Kornblith, S., Norouzi, M., and Hinton, G. A simple framework for contrastive learning of visual representations. In *ICML*, 2020.
- Chen, X., Xie, S., and He, K. An empirical study of training self-supervised vision transformers. In *ICCV*, 2021a.
- Chen, X., Xie, S., and He, K. An empirical study of training self-supervised vision transformers. In *ICCV*, 2021b.
- Chen, X., Ding, M., Wang, X., Xin, Y., Mo, S., Wang, Y., Han, S., Luo, P., Zeng, G., and Wang, J. Context autoencoder for self-supervised representation learning. *IJCV*, 2024.
- Cheng, Y. Mean shift, mode seeking, and clustering. *TPAMI*, 1995.
- Deng, J., Dong, W., Socher, R., Li, L.-J., Li, K., and Fei-Fei, L. ImageNet: A large-scale hierarchical image database. In *CVPR*, 2009.
- Dong, Y., Cordonnier, J.-B., and Loukas, A. Attention is not all you need: Pure attention loses rank doubly exponentially with depth. In *ICML*, 2021.
- Fischer, K., Dahmen, D., and Helias, M. Optimal signal propagation in ResNets through residual scaling. *arXiv:2305.07715*, 2023.
- Garrido, Q., Balestrieri, R., Najman, L., and Lecun, Y. Rankme: Assessing the downstream performance of pre-trained self-supervised representations by their rank. In *International conference on machine learning*, pp. 10929–10974. PMLR, 2023.
- Geshkovski, B., Letrouit, C., Polyanskiy, Y., and Rigollet, P. The emergence of clusters in self-attention dynamics. In *NeurIPS*, 2024.
- Glorot, X. and Bengio, Y. Understanding the difficulty of training deep feedforward neural networks. In *ICAIS*, 2010.
- Goodfellow, I., Pouget-Abadie, J., Mirza, M., Xu, B., Warde-Farley, D., Ozair, S., Courville, A., and Bengio, Y. Generative adversarial nets. In *NeurIPS*, 2014.
- Greff, K., Srivastava, R. K., and Schmidhuber, J. Highway and residual networks learn unrolled iterative estimation. In *ICLR*, 2017.
- Grill, J.-B., Strub, F., Altché, F., Tallec, C., Richemond, P., Buchatskaya, E., Doersch, C., Avila Pires, B., Guo, Z., Gheshlaghi Azar, M., et al. Bootstrap your own latent: A new approach to self-supervised learning. In *NeurIPS*, 2020.
- He, K., Zhang, X., Ren, S., and Sun, J. Deep residual learning for image recognition. In *CVPR*, 2016.
- He, K., Fan, H., Wu, Y., Xie, S., and Girshick, R. Momentum contrast for unsupervised visual representation learning. In *CVPR*, 2020.
- He, K., Chen, X., Xie, S., Li, Y., Dollár, P., and Girshick, R. Masked autoencoders are scalable vision learners. In *CVPR*, 2022.

- Ho, J., Jain, A., and Abbeel, P. Denoising diffusion probabilistic models. In *NeurIPS*, 2020.
- Hochreiter, S. and Schmidhuber, J. Long short-term memory. *Neural Computation*, 1997.
- Huang, G., Liu, Z., Van Der Maaten, L., and Weinberger, K. Q. Densely connected convolutional networks. In *CVPR*, 2017.
- Huang, Z., Jin, X., Lu, C., Hou, Q., Cheng, M.-M., Fu, D., Shen, X., and Feng, J. Contrastive masked autoencoders are stronger vision learners. *TPAMI*, 2023.
- Huh, M., Mobahi, H., Zhang, R., Cheung, B., Agrawal, P., and Isola, P. The low-rank simplicity bias in deep networks. *arXiv:2103.10427*, 2021.
- Ioffe, S. and Szegedy, C. Batch normalization: Accelerating deep network training by reducing internal covariate shift. In *ICML*, 2015.
- Jing, L., Zbontar, J., and LeCun, Y. Implicit rank-minimizing autoencoder. In *NeurIPS*, 2020.
- Karras, T., Aila, T., Laine, S., and Lehtinen, J. Progressive growing of GANs for improved quality, stability, and variation. In *ICLR*, 2018.
- Karras, T., Laine, S., and Aila, T. A style-based generator architecture for generative adversarial networks. *TPAMI*, 2021.
- Kingma, D. P. and Welling, M. Auto-encoding variational bayes. *arXiv:1312.6114*, 2013.
- Kirillov, A., Mintun, E., Ravi, N., Mao, H., Rolland, C., Gustafson, L., Xiao, T., Whitehead, S., Berg, A. C., Lo, W.-Y., Dollár, P., and Girshick, R. Segment anything. *arXiv:2304.02643*, 2023.
- Kojima, T., Gu, S. S., Reid, M., Matsuo, Y., and Iwasawa, Y. Large language models are zero-shot reasoners. In *NeurIPS*, 2022.
- Larsson, G., Maire, M., and Shakhnarovich, G. FractalNet: Ultra-deep neural networks without residuals. In *ICLR*, 2017.
- Laskar, M. T. R., Bari, M. S., Rahman, M., Bhuiyan, M. A. H., Joty, S., and Huang, J. X. A systematic study and comprehensive evaluation of ChatGPT on benchmark datasets. *arXiv:2305.18486*, 2023.
- Li, T., Chang, H., Mishra, S., Zhang, H., Katabi, D., and Krishnan, D. MAGE: Masked generative encoder to unify representation learning and image synthesis. In *CVPR*, 2023.
- Loshchilov, I. and Hutter, F. Decoupled weight decay regularization. In *ICLR*, 2019.
- Neyshabur, B., Li, Z., Bhojanapalli, S., LeCun, Y., and Srebro, N. Towards understanding the role of over-parameterization in generalization of neural networks. In *ICLR*, 2019.
- Radhakrishnan, A., Beaglehole, D., Pandit, P., and Belkin, M. Mechanism of feature learning in deep fully connected networks and kernel machines that recursively learn features. *arXiv:2212.13881*, 2022.
- Radhakrishnan, A., Belkin, M., and Drusvyatskiy, D. Linear recursive feature machines provably recover low-rank matrices. *arXiv:2401.04553*, 2024.
- Ramesh, A., Pavlov, M., Goh, G., Gray, S., Voss, C., Radford, A., Chen, M., and Sutskever, I. Zero-shot text-to-image generation. In *ICML*, 2021.
- Rombach, R., Blattmann, A., Lorenz, D., Esser, P., and Ommer, B. High-resolution image synthesis with latent diffusion models. In *CVPR*, 2022.
- Ronneberger, O., Fischer, P., and Brox, T. U-Net: Convolutional networks for biomedical image segmentation. In *MICCAI*, 2015.
- Roy, O. and Vetterli, M. The effective rank: A measure of effective dimensionality. In *ESPC*, 2007.
- Savarese, P. and Figueiredo, D. Residual gates: A simple mechanism for improved network optimization. In *ICLR*, 2017.
- Schuhmann, C., Beaumont, R., Vencu, R., Gordon, C., Wightman, R., Cherti, M., Coombes, T., Katta, A., Mullis, C., Wortsman, M., et al. LAION-5B: An open large-scale dataset for training next generation image-text models. In *NeurIPS*, 2022.
- Shi, Z., Zhou, X., Qiu, X., and Zhu, X. Improving image captioning with better use of captions. In *ACL*, 2020.
- Singh, M., Duval, Q., Alwala, K. V., Fan, H., Aggarwal, V., Adcock, A., Joulin, A., Dollár, P., Feichtenhofer, C., Girshick, R., et al. The effectiveness of MAE pre-pretraining for billion-scale pretraining. *arXiv:2303.13496*, 2023.
- Song, J., Meng, C., and Ermon, S. Denoising diffusion implicit models. In *ICLR*, 2021a.
- Song, Y., Sohl-Dickstein, J., Kingma, D. P., Kumar, A., Ermon, S., and Poole, B. Score-based generative modeling through stochastic differential equations. In *ICLR*, 2021b.
- Song, Y., Dhariwal, P., Chen, M., and Sutskever, I. Consistency models. In *ICML*, 2023.

- Srivastava, R. K., Greff, K., and Schmidhuber, J. Highway networks. *arXiv:1505.00387*, 2015a.
- Srivastava, R. K., Greff, K., and Schmidhuber, J. Training very deep networks. In *NeurIPS*, 2015b.
- Szegedy, C., Liu, W., Jia, Y., Sermanet, P., Reed, S., Anguelov, D., Erhan, D., Vanhoucke, V., and Rabinovich, A. Going deeper with convolutions. In *CVPR*, 2015.
- Team, G., Anil, R., Borgeaud, S., Wu, Y., Alayrac, J.-B., Yu, J., Soricut, R., Schalkwyk, J., Dai, A. M., Hauth, A., et al. Gemini: A family of highly capable multimodal models. *arXiv:2312.11805*, 2023.
- Tian, C., Tao, C., Dai, J., Li, H., Li, Z., Lu, L., Wang, X., Li, H., Huang, G., and Zhu, X. ADDP: Learning general representations for image recognition and generation with alternating denoising diffusion process. In *ICLR*, 2024.
- Vaswani, A., Shazeer, N., Parmar, N., Uszkoreit, J., Jones, L., Gomez, A. N., Kaiser, Ł., and Polosukhin, I. Attention is all you need. In *NeurIPS*, 2017.
- Wei, Y., Gupta, A., and Morgado, P. Towards latent masked image modeling for self-supervised visual representation learning. *arXiv preprint arXiv:2407.15837*, 2024.
- Wu, Z., Xiong, Y., Yu, S. X., and Lin, D. Unsupervised feature learning via non-parametric instance discrimination. In *CVPR*, 2018.
- Yang, X. and Wang, X. Diffusion model as representation learner. In *ICCV*, 2023.
- Yi, K., Ge, Y., Li, X., Yang, S., Li, D., Wu, J., Shan, Y., and Qie, X. Masked image modeling with denoising contrast. In *ICLR*, 2023.
- Zhang, X., Yunis, D., and Maire, M. Deciphering ‘what’ and ‘where’ visual pathways from spectral clustering of layer-distributed neural representations. In *CVPR*, 2024.
- Zhou, J., Wei, C., Wang, H., Shen, W., Xie, C., Yuille, A., and Kong, T. iBOT: Image BERT pre-training with online tokenizer. In *ICLR*, 2022.
- Zhu, L., Deng, R., Maire, M., Deng, Z., Mori, G., and Tan, P. Sparsely aggregated convolutional networks. In *ECCV*, 2018.

A. Training and Evaluation Details

A.1. Model training.

Our training configurations primarily followed the guidelines established by He et al. (2022). In the ImageNet-1K experiment, our model was trained for 800 epochs, utilizing the AdamW (Loshchilov & Hutter, 2019) optimizer with a constant weight decay of $5e-2$ for a batch size of 1024. We set the maximum learning rate to $6e-4$. Initially, the learning rate started at 0 and linearly increased to its maximum over the first 40 epochs, after which it followed a cosine schedule to gradually decrease to zero by the end of the training period. It is worth noting that the learning rate per sample, or effective learning rate, in our setup matched that of He et al. (2022), although our maximum learning rate was set lower due to our batch size being a quarter of theirs. We applied random resizing, cropping, and horizontal flipping during training as part of our augmentation scheme. To enhance the quality of the learned representations in most experiments, we employed the normalized pixel loss, as proposed by (He et al., 2022). In the ImageNet-100 experiment, we employed the identical training configuration used in the ImageNet-1K experiments. We train our model with 4 NVIDIA A40 GPUs and a completed training usually takes 20 hours on ImageNet-100 and 200 hours on ImageNet-1k.

A.2. Evaluation with Linear Probing.

For the ImageNet-1k dataset, we use the exact same evaluation protocols employed in He et al. (2022), which includes random data augmentation.

For the ImageNet-100 dataset, we employed a simpler evaluation protocol: We train the linear classifier with a batch size of 1024 for 200 epochs, where the learning rate starts at $1e-2$ and then decays towards 0 using a cosine scheduler. During this evaluation, we do not apply any data augmentation.

A.3. Modified Architecture

We present a visualization of our UNet transformer design, as outlined in Section 3.2, in Fig. 5. It’s important to note that decayed identity shortcuts are exclusively implemented within the encoder block. Additionally, we establish skip connections from alternating blocks in the encoder to the decoder, following the UNet (Ronneberger et al., 2015) architecture’s design principles.

A.4. Learnable α_l over network layers

In the ablation study of learnable α_l , we apply no additional regularization beyond standard weight decay to the model parameters. Table 5 presents the α_l values for each layer. The results do not reveal any meaningful pattern across network depth.

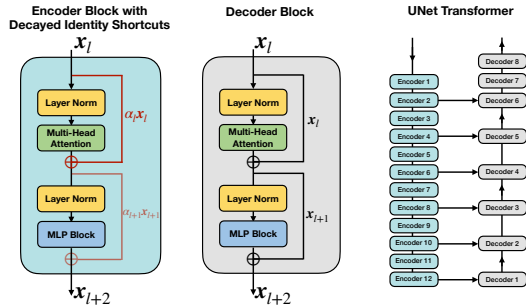


Figure 5. We present our enhanced UNet Transformer architecture for Masked Auto-encoder. (1) **Left**: Our customized encoder blocks, equipped with our proposed decay identity shortcuts. (2) **Middle**: Standard transformer blocks as the decoder blocks. (3) **Right**: We incorporate the decay identity shortcuts exclusively within the encoder blocks of our UNet transformer and employ standard transformer blocks for the decoder. To support abstract representation learning at the bottleneck, *i.e.*, the last layer of the Encoder 12, we adopt the UNet (Ronneberger et al., 2015) architecture and create skip connections that transmit every other encoder feature directly to the decoder.

B. Further experiments

B.1. Reconstruction quality.

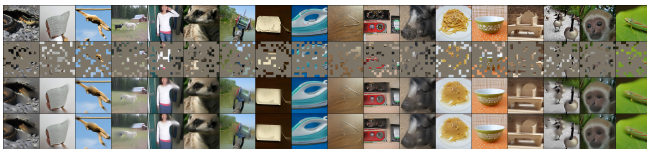


Figure 6. **Qualitative comparison of images reconstructed by MAE with and without our method.** We observe our method learns features with higher linear probing accuracy without compromising reconstruction quality. Row 1: ground truth test image. Row 2: images masked at 75%. Row 3: reconstructions with our method. Row 4: reconstructions with baseline MAE.

We qualitatively evaluate test images reconstructed by an MAE using our framework and images reconstructed by the original MAE. We show the reconstructed images in Figure 6. While the focus of our work is entirely to improve the representations learned by an encoder, we observe that our framework does not harm the reconstructions. Hence, there is no qualitative tradeoff for our increase in linear probing accuracy.

B.2. Abstraction and Low-rank in the Supervised Setting

In this experiment, we modify the standard ResNet-18 model to experiment with different depth models. By default, the ResNet-18 has a total of 8 residual blocks that are equally distributed into 4 layers. To increase model depth,

Residual Connections Harm Generative Representation Learning

Layer Index	1	2	3	4	5	6	7	8	9	10	11	12
Attention	0.993	0.947	0.982	0.766	0.992	0.795	0.988	0.849	0.998	0.723	0.811	0.488
FFN	0.989	0.926	0.961	0.620	0.961	0.442	0.711	0.322	0.810	0.475	0.637	0.353

Table 5. Learnable α_l values for different model layers. In contrast to our proposed linear scheduler, learnable α_l does not exhibit a consistent decay pattern across network depth.

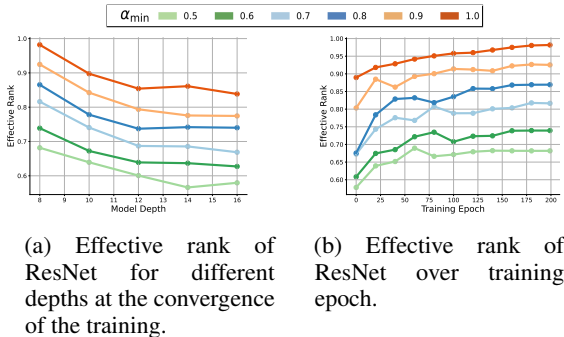


Figure 7. Dynamics of the feature rank in the supervised setup.

We train ResNet models for a supervised classification task on a small subset of ImageNet. And visualize (a) effective rank across different depths at convergence and (b) training dynamics of effective rank over time for various α_{min} . In (a) we see that at convergence, our method consistently decreases the feature rank with various depth and, in (b), this pattern is also shown for standard ResNet model at every stage of training.

we repeat residual blocks in the 3rd layer to obtain models varying between 8 and 16 total layers. At convergence, we observe that the models of different depths achieve a similar test accuracy. However, despite similar accuracies, in Figure 7a, which visualizes the effective rank over depth for different values of α_{min} , we see that the effective rank decreases over depth. Furthermore, smaller values of α_{min} consistently lead to features with lower effective rank.

Next, in Figure 7b, we try to verify our conjecture by visualizing the evolution of effective rank during training when choosing different α_{min} in our method. For this experiment, we choose to train the standard ResNet-18 using our decayed identity shortcuts. In this setup, we observe that the optimal choice of α_{min} slightly improves the test accuracy of the classification network: 94.4% with $\alpha_{min} = 0.7$ vs. 93.6% with $\alpha_{min} = 1.0$. We observe that the effective rank of the final features decreases with decreasing α_{min} . This supports our hypothesis that (1) decayed identity shortcuts substantially decrease the rank of bottleneck features and (2) decreasing feature rank may help improve learned features.

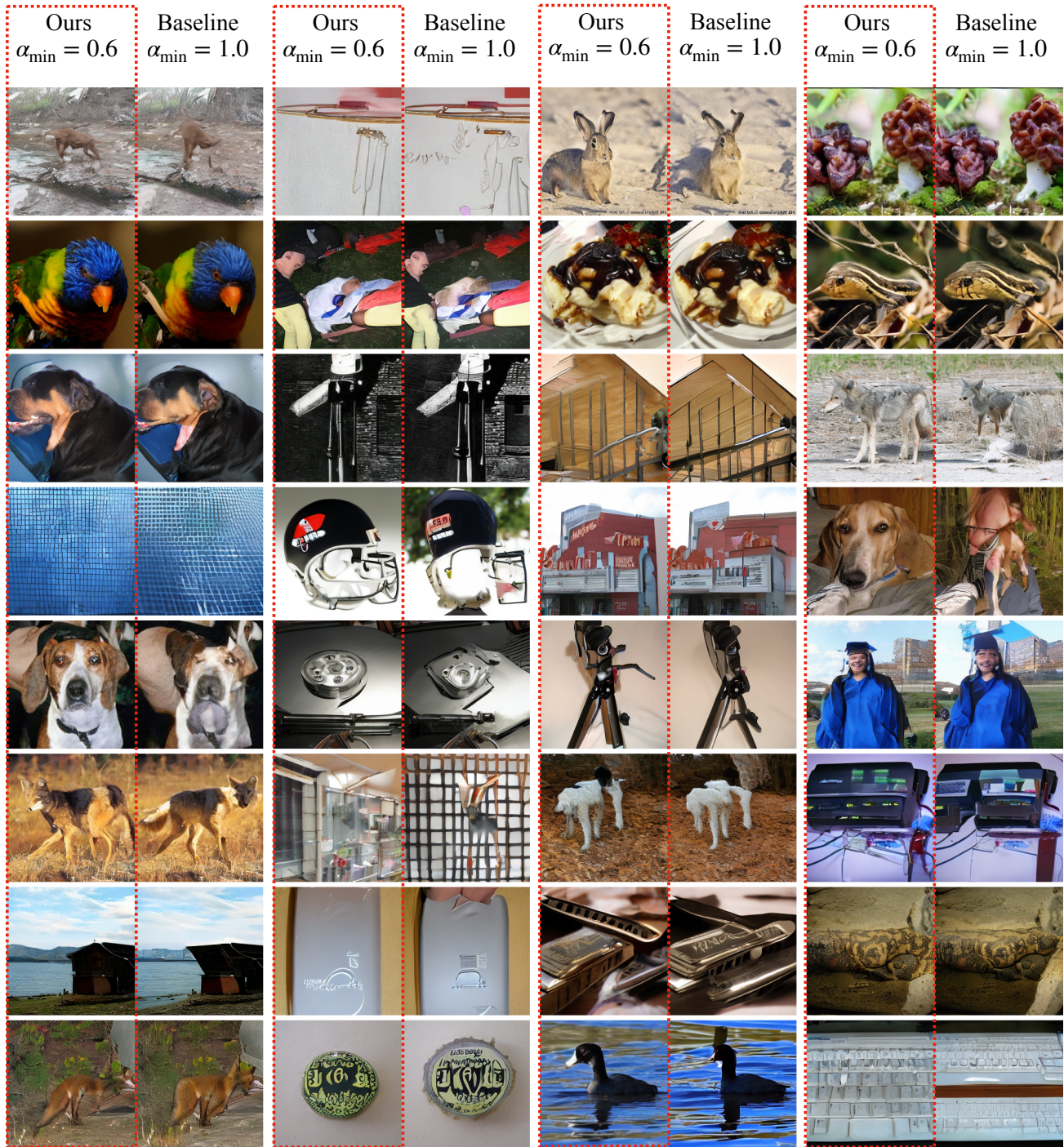


Figure 8. Qualitative comparison of images generated by diffusion models. Our method, decayed identity shortcuts with $\alpha_{\min} = 0.6$, shows improved representation learning and produces higher-quality generated images compared to the baseline, which employs full residual connections ($\alpha_{\min} = 1.0$).